




Impact of halide anions on ionic transport and thermoelectric properties of polyvinyl alcohol-based eutectogel

Yu-Syuan Jheng^a, Ching-Chieh Hsu^a, Shao-Huan Hong^a, Chi-Wei Hsu^a, Shiao-Wei Kuo^b, Chia-Hsin Wang^c, U-Ser Jeng^c, Shih-Huang Tung^{a,d}, Cheng-Liang Liu^{a,d,e,*} 

^a Department of Materials Science and Engineering, National Taiwan University, Taipei, 10617, Taiwan

^b Department of Materials and Optoelectronic Science, Center of Crystal Research, National Sun Yat-Sen University, Kaohsiung, 80424, Taiwan

^c National Synchrotron Radiation Research Center, Hsinchu, 30076, Taiwan

^d Institute of Polymer Science and Engineering, National Taiwan University, Taipei, 10617, Taiwan

^e Advanced Research Center for Green Materials Science and Technology, National Taiwan University, Taipei, 10617, Taiwan

ARTICLE INFO

Keywords:

Biocompatible
Thermoelectric
Eutectogel
Hydrogen bond acceptor
Wearable device

ABSTRACT

An environmentally friendly eutectogel (ETG) based on polyvinyl alcohol (PVA) and glycerol-based deep eutectic solvents (DESs) is developed without chemical crosslinkers. Unlike most previous studies that exclusively employed choline chloride (ChCl) as the hydrogen bond acceptor (HBA), this work systematically investigates three different HBAs, namely choline chloride (ChCl), choline bromide (ChBr), and choline iodide (ChI), whose anions possess distinct chaotropic properties. Among them, Γ^- , exhibiting the strongest chaotropic effect, disrupts the hydrogen-bonding network and lowers the crystallinity of the PVA matrix. The thermoelectric properties are mainly determined by DES viscosity, ion-polymer binding energy, and steric effects from ionic size. Of the three, the Br^- -based ETG achieves the highest ionic conductivity (63.33 mS cm^{-1}), thermopower (5.70 mV K^{-1}), and ionic figure of merit (0.14), owing to its optimal balance of moderate halide-polymer interactions, low viscosity, and small ionic radius. This comparative study expands the scope of HBAs beyond conventional ChCl, providing new design principles and broader material choices for thermoelectric gels in sustainable and wearable energy-harvesting.

1. Introduction

The rising global energy demand and growing environmental concerns have highlighted the importance of developing technologies that are capable of harvesting low-grade waste heat and converting it into useable energy [1–3]. Traditional inorganic thermoelectric materials such as PbTe and Bi_2Te_3 , and SiGe alloys were first explored in the mid-20th century for their moderate thermopowers ($\sim 200 \text{ } \mu\text{V K}^{-1}$). These materials offer good electrical conductivity, but their applications are limited by brittleness, toxicity, and high fabrication costs [4]. These limitations have prompted a shift toward more sustainable, flexible, and eco-friendly alternatives that are suitable for wider applications. Among the emerging candidates, ionic thermoelectric materials present several key advantages, including low density, non-toxicity, low thermal conductivity, and high tunable thermopower values [5,6]. In contrast to conventional electron-based thermoelectric materials, the ionic materials operate via thermal gradient-driven ion migration, a phenomenon

known as the Soret effect [7–9]. In this process, ions accumulate at the electrodes under a temperature gradient, where they effectively generate a thermovoltage by acting as a thermally charged capacitor [10,11]. This distinct mechanism has sparked growing interest in soft, flexible systems—especially gel-based ionic thermoelectric systems, which combine polymeric gels with ionic species to create highly adaptable platforms for energy harvesting.

In recent years, polyvinyl alcohol (PVA) has emerged as an attractive material for flexible electronics and biomaterials due to its biocompatibility, low cytotoxicity, good film-forming ability, and favorable mechanical properties [12]. In ionic thermoelectric system, PVA is frequently used to encapsulate ionic liquids or salts within a hydrogel network. These PVA-based hydrogels are often chemically crosslinked using agents such as boric acid, glutaraldehyde, or formaldehyde to enhance mechanical strength and thermal stability [13,14]. However, residual crosslinking agents may pose cytotoxicity risks, particularly for wearable or biomedical applications [15]. Therefore, the development

* Corresponding author. Department of Materials Science and Engineering, National Taiwan University, Taipei, 10617, Taiwan.

E-mail address: liucl@ntu.edu.tw (C.-L. Liu).

<https://doi.org/10.1016/j.mtener.2025.102105>

Received 9 September 2025; Received in revised form 10 October 2025; Accepted 15 October 2025

Available online 17 October 2025

2468-6069/© 2025 Elsevier Ltd. All rights are reserved, including those for text and data mining, AI training, and similar technologies.

of environmentally friendly and non-toxic crosslinking strategies remains a critical challenge in advancing design of ionic thermoelectric materials. In addition to optimizing the polymer matrix, the choice of ionic charge carriers is crucial for enhancing thermoelectric performance. Ionogels, which combine ionic liquids with polymer matrices, have shown promising potential due to their inherently high thermopower. For instance, Cheng et al. reported an ionogel based on poly(vinylidene fluoride)-hexafluoropropylene (PVDF-HFP) and 1-ethyl-3-methylimidazolium dicyanamide (EMIM:DCA), achieving a thermopower of 26.1 mV K^{-1} [16]. Similarly, Zhao et al. developed an ionogel comprised of polyethylene oxide (PEO), lithium bis(trifluoromethanesulfonyl)imide (LiTFSI), and 1-ethyl-3-methylimidazolium tetrafluoroborate (EMIM:BF₄), yielding a thermopower of -15 mV K^{-1} [17]. However, despite their high performance, ionic liquids face limitations such as high toxicity, elevated cost, and complex synthesis. To address these challenges, deep eutectic solvents (DESs) have emerged as sustainable alternatives to conventional ionic liquids. A DES is typically formed by complexing a hydrogen bond donor (HBD) with a hydrogen bond acceptor (HBA), producing a eutectic mixture with a melting point far below that of each individual component [18]. The typical DES exhibits many favorable properties in common with ionic liquids, such as high ionic conductivity, low volatility, and thermal stability, while offering additional advantages such as lower toxicity, improved biocompatibility, and facile economical synthesis from readily available precursors [19,20]. These features make DESs particularly ideal candidates for next-generation, environmentally friendly ionic thermoelectric systems, particularly in wearable electronics.

Recent studies have demonstrated the potential of thermoelectric eutectogel (ETG) systems incorporating DESs as ionic thermoelectric materials. For instance, Zhao et al. reported ETGs based on waterborne polyurethane (WPU) and DES systems such as choline chloride:ethylene glycol (ChCl:EG), choline chloride:glycerol (ChCl:Gly), and choline chloride:urea (ChCl:Urea), to achieve thermopowers of 15.9, 13.4, and 12.1 mV K^{-1} , respectively [21]. Similarly, Chen et al. developed cellulose nanofiber (CNF)-based ETGs using ChCl:EG and ChCl:Urea, to achieve thermopowers of 17.96 and 9.27 mV K^{-1} , respectively [22]. While these studies highlight the tunability of performance via the choice of HBD, the selection of a HBA has thus far remained largely confined to ChCl. Therefore, an exploration of HBAs represents an important direction for further improving the performance and versatility of thermoelectric ETGs.

In the present study, a PVA-based ETG system is prepared without the need for chemical crosslinkers, thereby ensuring low toxicity, environmental sustainability, and suitability for wearable applications. Glycerol is selected as the HBD to form a DES system. Due to the poor compatibility between PVA and glycerol, the PVA chains adopt a folded conformation within the gel, which enhances the mechanical strength of the network. To systematically explore the influence of the HBA, three halide-based HBAs are selected, namely: choline chloride (ChCl), choline bromide (ChBr), and choline iodide (ChI). The aim of this study is to identify viable alternatives to the widely used ChCl, with the goal of optimizing both the thermoelectric performance and environmental sustainability. Thus, the chaotropic nature of the selected halide anion is found to significantly affect the solvent microstructure and polymer chain conformation, while variations in viscosity and ionic size across the DES systems lead to pronounced differences in thermoelectric performance. Among the tested systems, the ChBr-based ETG (designated as ETG-Br) exhibits the better performance, achieving an ionic conductivity of 63.33 mS cm^{-1} and a thermopower of 5.70 mV K^{-1} . As summarized in Table S2, the results indicate that the crosslinker-free ETG obtained by the introduction of the ETG-Br HBA can achieve a comparable performance to that of typical ETGs with crosslinkers. Further, when this optimized material is used to fabricate an ionic thermoelectric capacitor, an energy density of 2.3 mJ m^{-2} is demonstrated. For practical demonstration, the ETG-Br is integrated into a wearable thermoelectric device that harvests body heat from the human wrist under

ambient conditions. With a modest temperature gradient of only 6 K, the device generates an output voltage of 32.0 mV. In brief, the superior electrochemical and thermoelectric performance of ChBr not only surpasses that of the commonly used ChCl, but also retains the environmental friendliness, safety, and ease of preparation inherent to DES-based systems. These findings demonstrate that tuning the halide-based HBA composition enables a balanced enhancement of ionic conductivity and thermopower, providing a sustainable and promising strategy for developing environmentally friendly DES-based ionic thermoelectric materials.

2. Experimental

2.1. Materials

Poly(vinyl alcohol) (PVA, $M_w \sim 146000\text{--}186000$, 99+% hydrolyzed) was obtained from Sigma-Aldrich. Choline chloride (ChCl, >98.0 %), choline bromide (ChBr, >98.0 %) and choline iodide (ChI, >98.0 %) were purchased from Tokyo Chemical Industry. Glycerol (C₃H₈O₃, 99.0 %) was obtained from Showa Chemical Industry Co., Ltd. All chemicals were used as received without further purification.

2.2. Sample preparation

To prepare the eutectogel, 1.36 g of PVA powder was dissolved in 10 mL of deionized water and stirred at 90 °C for 5 h to obtain a 12 wt% PVA solution. Deep eutectic solvents (DES) were then prepared by mixing choline salts (ChCl, ChBr, or ChI) with glycerol at a molar ratio of 1:2. To further lower the eutectic point, 15 wt% of deionized water was added to the mixture, which was stirred at 65 °C for 1 h. The resulting DES was then combined with the PVA solution at a weight ratio of 1:2 and stirred at 90 °C for 1 h. The mixture was poured into PTFE molds and allowed to cool to room temperature. A single freeze-thaw cycle was applied to the mixture, consisting of freezing at -15 °C for 20 h followed by thawing at room temperature for 5 h, to form a stable eutectogel. The synthesis procedure of the eutectogel is illustrated in Fig. S1, and the detailed compositions of the eutectogels are listed in Table S1.

2.3. Ionic thermoelectric characterization

The ionic conductivity (σ_i) of the eutectogels was determined by placing the samples between two platinum electrodes, with the bulk resistance (R) measured via electrochemical impedance spectroscopy (EIS) using a BioLogic SP-50e system. The σ_i was calculated using the equation $\sigma_i = l/(R \times A)$, where l is the thickness of the eutectogels and A is the cross-sectional contact area. Thermopower (S_i) was measured using a custom-assembled setup featuring platinum electrodes ($1.5 \times 1.5 \text{ cm}^2$) attached to the upper and lower surfaces of the sample holder. The measurement was conducted in a relatively enclosed chamber with the relative humidity of 30 %. A temperature gradient between 20 °C and 40 °C was applied across the sample, and the corresponding thermoelectric voltage (ΔV) was recorded using a Keithley 2400A source-meter. Thermal conductivity measurements were conducted using the transient plane source (TPS) technique, employing a Hot Disk TPS 2500S thermal analyzer to determine the heat transport properties of the samples.

3. Results and discussion

3.1. Design and synthesis of thermoelectric eutectogels

To advance the development of eco-friendly ETGs for wearable thermoelectric applications, PVA was used as the polymer matrix, while the use of chemical crosslinkers was deliberately avoided in order to preserve the material's environmental sustainability. Glycerol was selected for its dual function as the HBD and as a poor solvent for PVA,

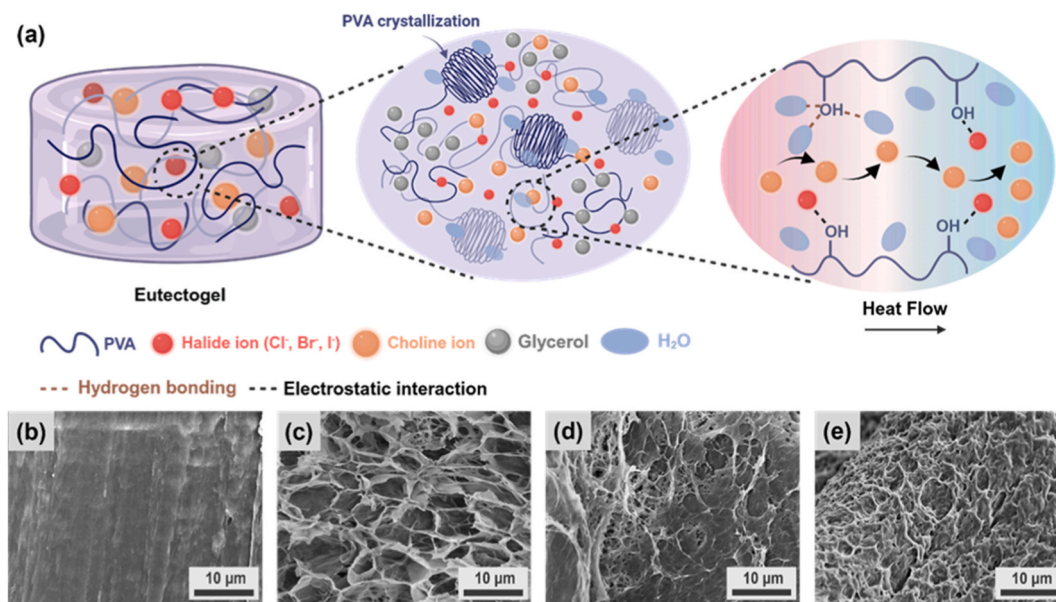


Fig. 1. (a) Schematic illustration of the eutectogel structures. A magnified view reveals partial phase separation between glycerol and water domains within the matrix, with further zoom-in highlighting the ion transport mechanism enabled by localized interactions among halide ions, water molecules, and polymer chains. SEM images of (b) PVA hydrogel, (c) ETG-Cl, (d) ETG-Br, and (e) ETG-I, highlighting morphological differences induced by halide variation.

thereby inducing partial folding of the PVA polymer chains within water-rich domains. In turn, these folded regions acted as physical crosslinking points, thereby enhancing the mechanical robustness of the gel network [23]. Meanwhile, DESs were selected as an alternative to conventional ionic liquids, which are often limited by toxicity concerns and synthetic complexity. While previous studies on thermoelectric ETGs have largely focused on tuning the composition of the HBD components, the effects of varying the HBA composition remain comparatively underexplored. To address this knowledge gap, a series of DES formulations was selected for the present study, including choline chloride (ChCl), choline bromide (ChBr), and choline iodide (ChI), each paired with glycerol. The aim of this study is to identify viable HBA alternatives to the widely used ChCl, with the goal of optimizing both the thermoelectric performance and environmental sustainability [24–26].

As illustrated in Fig. S1 of the Supplementary Material and described in detail in the Experimental Section, ETGs were synthesized by blending an aqueous PVA solution with various DESs, including ChCl:Gly, ChBr:Gly, and ChI:Gly, at a PVA:DES weight ratio of 2:1. Each mixture was stirred at 90 °C for 1 h and subsequently subjected to a single freeze-thaw cycle. The resulting materials were designated as

ETG-Cl, ETG-Br, and ETG-I, respectively, based on the halide species used. For reference, a pure PVA hydrogel was also prepared under identical thermal conditions but without the addition of DES. As shown schematically in Fig. 1(a), the addition of the glycerol-based DES into the PVA matrix triggers microphase separation, which is primarily driven by the contrasting solvation behavior of PVA in water and glycerol. While water acts as a good solvent for PVA, glycerol is a comparatively poor solvent, thus leading to preferential aggregation and crystallization of PVA chains within water-rich domains. These discrete crystalline regions serve as physical crosslinking points, reinforcing the gel network and enhancing the mechanical robustness of the ETGs [23]. The addition of chaotropic ions disrupts the intrinsic hydrogen-bonding network of water, thereby diminishing its tendency to maintain an ordered structure and weakening the hydrophobic effect of the DES. This suppression of water structuring reduces the aggregation of hydrophobic domains within the PVA matrix and weakens the intermolecular associations between PVA chains. As a result, the polymer adopts a more extended conformation with greater exposure of hydroxyl groups. From a thermoelectric perspective, the electrostatic interactions between halide anions and PVA hydroxyl groups hinder the anion mobility relative to that of the more mobile choline cations, thereby affecting the

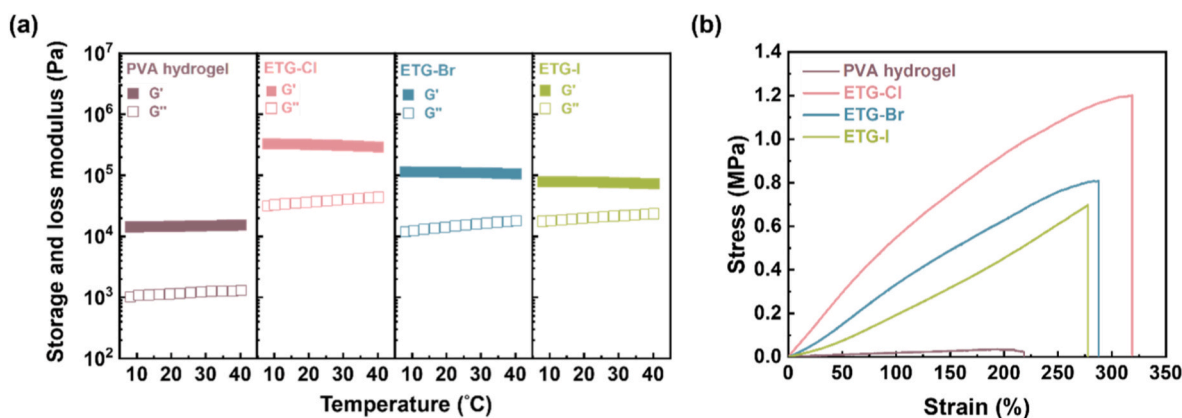


Fig. 2. Mechanical properties of the PVA hydrogel and eutectogels. (a) Rheological behavior as a function of temperature (20–40 °C). (b) Stress-strain curves of the samples.

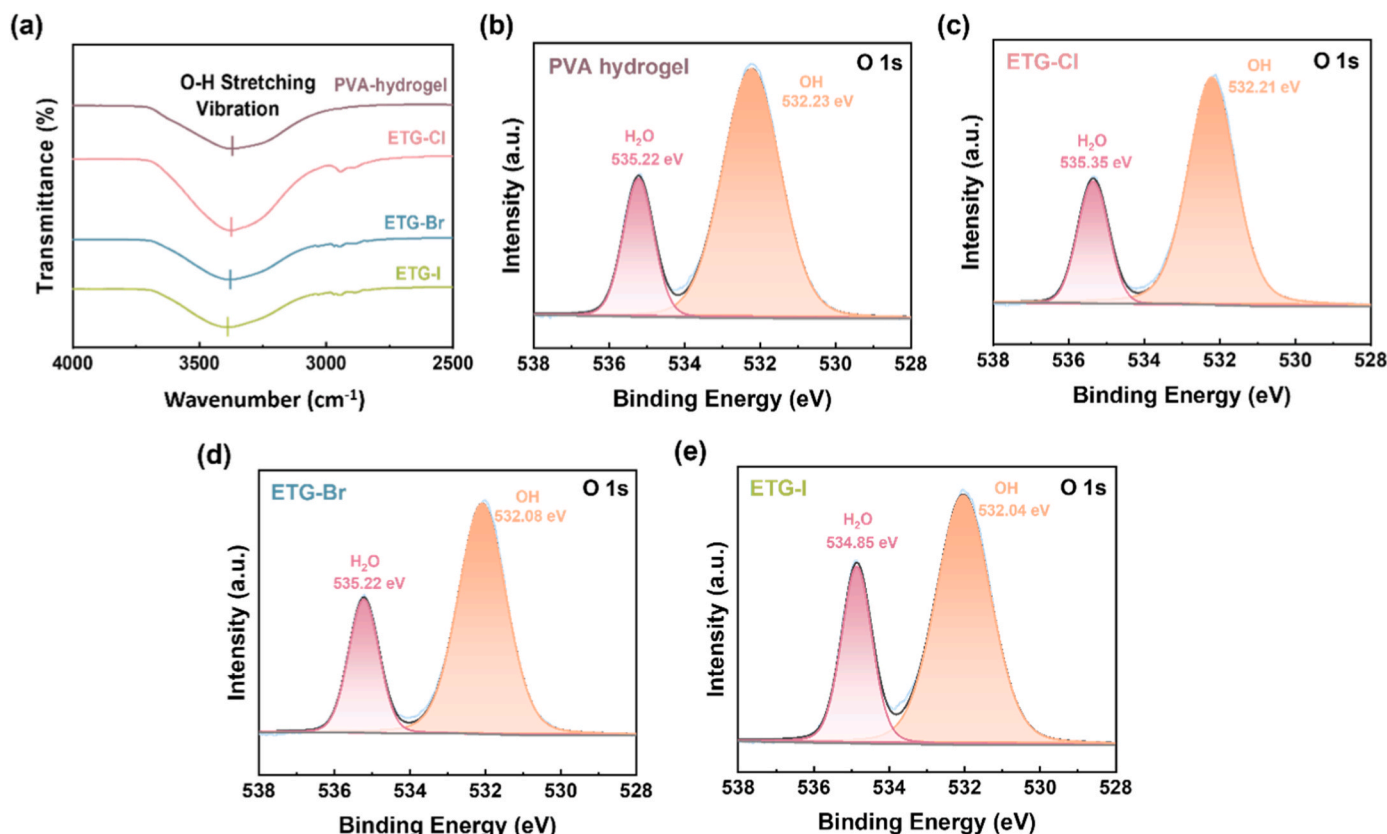


Fig. 3. (a) FTIR spectra of the PVA hydrogel and eutectogels. XPS spectra of (b) PVA hydrogel, (c) ETG-Cl, (d) ETG-Br, and (e) ETG-I.

selective ion transport that governs the thermodiffusion behavior. Under an applied thermal gradient, this disparity in ionic mobility drives the preferential thermodiffusion of positive charge carriers, thereby yielding p-type thermoelectric behavior in the ETGs.

The microstructural features of the prepared ETGs are revealed by the scanning electron microscopy (SEM) images in Fig. 1(b–e). The pristine PVA hydrogel (Fig. 1(b)) displays a dense and compact morphology with a smooth surface, which is characteristic of uniform polymer chain entanglement and crystallization. By contrast, the ETG-Cl (Fig. 1(c)) exhibits a more open, layered morphology featuring an interconnected porous network. This type of morphology is known to promote uniform mechanical stress distribution, thereby enhancing both elasticity and toughness [27]. Notably, the microstructure becomes increasingly irregular with the incorporation of heavier halide ions. Thus, the ETG-Br (Fig. 1(d)) exhibits a more heterogeneous and disordered porous morphology, which is indicative of less uniform phase separation and crystallization, while the ETG-I (Fig. 1(e)) exhibits clearly defined closed-pore structures that clearly contrast with the more open and interconnected porous networks of the lighter halide-based ETGs. For a clearer comparison, the corresponding pore size distribution statistics derived from SEM images have been provided in Fig. S2, which further quantify the morphological differences and pore uniformity among the ETGs. These variations in microstructure, driven by the nature of the halide ion, are expected to directly influence the mechanical properties of the ETGs.

3.2. Mechanical property analysis

The structural robustness and flexibility of the as-prepared gels under conditions relevant to thermoelectric operation are demonstrated by the rheological and uniaxial tensile test results in Fig. 2. Thus, the rheological profiles over the temperature range of 20–40 °C (Fig. 2(a)) indicate quasi-solid-state behavior for all samples. This is evidenced by

the storage modulus (G') being consistently greater than the corresponding loss modulus (G''), which is indicative of an elasticity-dominated mechanical response [28–30]. Quantitatively, the pristine PVA hydrogel exhibits a G' value of 14.3 kPa, whereas the incorporation of a DES leads to a significant enhancement in mechanical rigidity, with increased G' values of 329.7, 113.6, and 78.5 kPa for the ETG-Cl, ETG-Br, and ETG-I, respectively. These pronounced increases in the storage modulus reflect the reinforcing effects imparted by the DES components, particularly the glycerol-halide combinations. Similarly, the uniaxial tensile test results in Fig. 2(b) reveal a dramatic increase in maximum tensile stress, from 22.6 kPa for the PVA hydrogel to 1201.8, 807.1, and 697.8 kPa for the ETG-Cl, ETG-Br, and ETG-I, respectively. These results highlight the outstanding mechanical strength achieved in the ETGs [31,32]. Additionally, all samples also exhibited extensibility, with strain-at-break values of 218.5 % (PVA hydrogel), 318.7 % (ETG-Cl), 287.5 % (ETG-Br), and 277.7 % (ETG-I).

The enhanced mechanical performance of the ETGs can be primarily attributed to the presence of glycerol in the DES, which induces microphase separation within the aqueous PVA matrix. This phase behavior promotes the folding and crystallization of PVA chains in water-rich regions, thereby forming physical crosslinking domains that strengthen the gel network [33]. Moreover, the type of halide anion plays a critical role in determining the mechanical properties of the ETGs. Consistently with the above SEM observations, the ETG-Cl exhibits a well-organized, interconnected porous microstructure that promotes uniform mechanical stress transfer, thereby enhancing its tensile strength and toughness. By contrast, the ETG-Br presents a more heterogeneous and discontinuous porous morphology, thereby limiting uniform stress distribution and resulting in lower mechanical reinforcement relative to the ETG-Cl. Similarly, the ETG-I contains closed, irregular domains that further impede the effective distribution of mechanical stress and impair the formation of a robust crosslinked network, which further reduces its capacity to sustain mechanical loads.

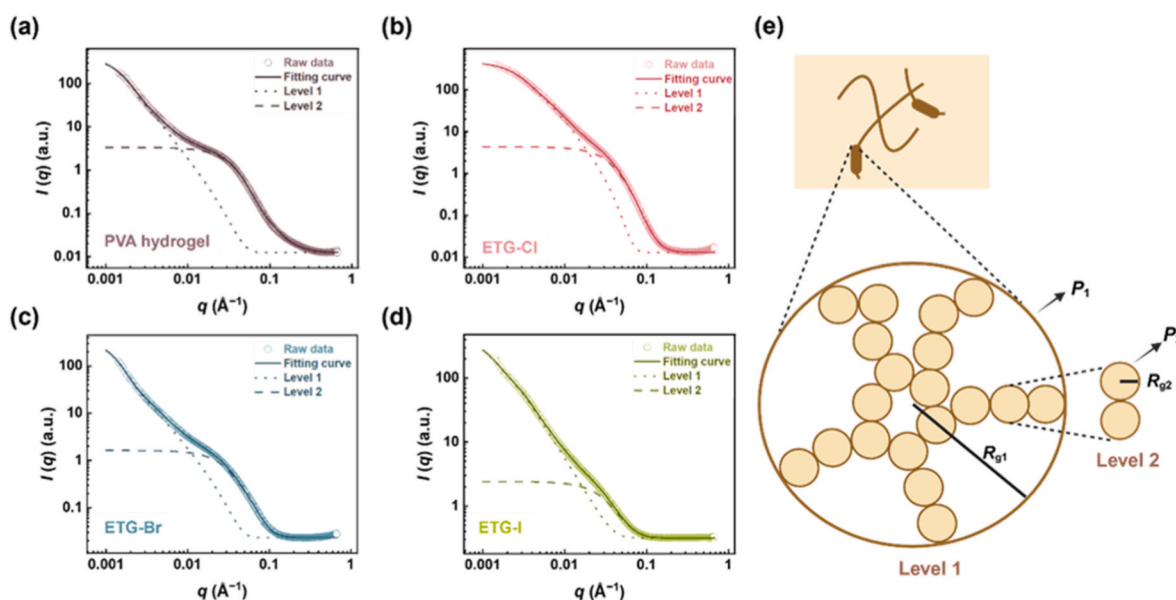


Fig. 4. SAXS profiles of (a) PVA hydrogel, (b) ETG-Cl, (c) ETG-Br, and (d) ETG-I. (e) Schematic illustration of the hierarchical polymer agglomerate structure, indicating two distinct levels of organization characterized by radii of gyration R_{g1} and R_{g2} .

In brief, the incorporation of a DES into the PVA hydrogel matrix dramatically improves the mechanical properties of the resulting ETGs. The combination of high tensile strength, large elongation at breaking point, and elasticity-dominated rheological behavior demonstrates that these gels can effectively withstand mechanical deformation while maintaining structural integrity. These favorable balanced mechanical characteristics are particularly advantageous for applications in flexible electronics and wearable devices, where mechanical durability and conformability are critical performance requirements.

3.3. Spectroscopic and structural characterization

The molecular-level interactions between the DES and PVA matrix are elucidated by the following Fourier-transform infrared spectroscopy (FTIR), X-ray photoelectron spectroscopy (XPS) and X-ray diffraction (XRD) results. These complementary techniques make it possible to examine how the various halide anions affect the hydrogen bonding network and electronic environment of hydroxyl groups within the PVA backbone. First, the FTIR spectra of the pristine PVA hydrogel and various ETGs in the wavenumber range of $4000\text{--}1000 \text{ cm}^{-1}$ are presented in Fig. S3, while an enlarged view in the narrower range of $4000\text{--}2500 \text{ cm}^{-1}$ is presented in Fig. 3(a) to facilitate a clearer comparison of the O-H stretching region. Thus, all samples exhibit a broad absorption band corresponding to the hydroxyl (O-H) stretching vibrations originating from both the water molecules and PVA, and this band undergoes a systematic blue shift from 3370.0 cm^{-1} for the pristine PVA hydrogel to 3373.6 , 3378.1 , and 3388.1 cm^{-1} for the ETG-Cl, ETG-Br, and ETG-I, respectively (Fig. 3(a)). These shifts indicate a progressive weakening of hydrogen-bonding interactions involving hydroxyl groups due to the increasing chaotropic nature of the halide anions ($\text{Cl}^- < \text{Br}^- < \text{I}^-$). The more chaotropic anions (Br^- and I^-) disrupt the water's hydrogen-bonding network, thereby suppressing the formation of a hydration shell around the hydrophobic regions of the PVA. This weakens the hydrophobic effect of the DES, thus leading to more expanded polymer chains and reduced intermolecular hydrogen bonding. This, in turn, leads to higher O-H stretching frequencies [34]. Conversely, in the pristine PVA hydrogel, abundant hydroxyl groups enable the formation of a dense and entangled hydrogen-bonding network. The incorporation of halide anions with low hydration enthalpies destabilizes this network by weakening the water-water interactions and promoting solvation of

the PVA by free water. As a result, the polymer chains adopt a more expanded conformation, as previously reported in systems with chaotropic additives that disrupt supramolecular order [35–37].

The changes in local chemical environment are further confirmed by the XPS results in Fig. S4 and S5. Specifically, the full survey spectra in Fig. S4 confirm the presence of C, O, and the corresponding halide ions, while the halogen-specific core-level spectra in Fig. S5 confirm the successful incorporation of Cl^- , Br^- , and I^- into the gel matrices during synthesis. Further, the O 1s core-level spectra of the various ETG samples are presented in Fig. 3(b–e), where a systematic shift in binding energy is observed, from 532.23 eV for the pristine PVA to 532.21 , 532.08 , and 532.04 eV for the ETG-Cl, ETG-Br, and ETG-I, respectively. The largest shift is observed in the ETG-I, which suggests the most pronounced alteration in the local electronic environment, and is consistent with a decrease in hydrogen-bonding participation by the oxygen atoms and a corresponding increase in local electron density.

The effect of DES incorporation on the long-range structural ordering is revealed by the XRD results in Fig. S6. There, the pristine PVA hydrogel exhibits a prominent diffraction peak at $2\theta \sim 28.1^\circ$, which is attributed to the (200) plane of the semi-crystalline domains, along with a minor peak at $2\theta \sim 41.1^\circ$, associated with secondary packing or minor crystalline inclusions [38]. Upon DES incorporation, the intensity of the primary diffraction peak decreases and shifts slightly toward lower angles, thereby indicating reduced crystallinity and increased interplanar spacing. This effect is most pronounced for the ETG-I, followed by the ETG-Br and ETG-Cl, which is consistent with the relative chaotropic capacities for the disruption of hydrogen bonding and ordered packing.

Taken together, the above FTIR, XPS, and XRD results reveal that chaotropic halide anions disrupt the hydrogen bonding and hydration shells of water around the PVA, thereby reducing the hydrophobic effect of the DES. This leads to chain expansion, along with weakening of the hydroxyl interactions and alterations in the polymer conformation and electronic environment. In particular, the I^- , possessing the strongest chaotropic character among the halides, induces the most significant structural rearrangement and disorder in the polymer network of ETG-I. These molecular-level insights demonstrate the critical role of halide anion identity in shaping the microenvironment of the ETG network, thereby influencing the mechanical properties of the resulting materials.

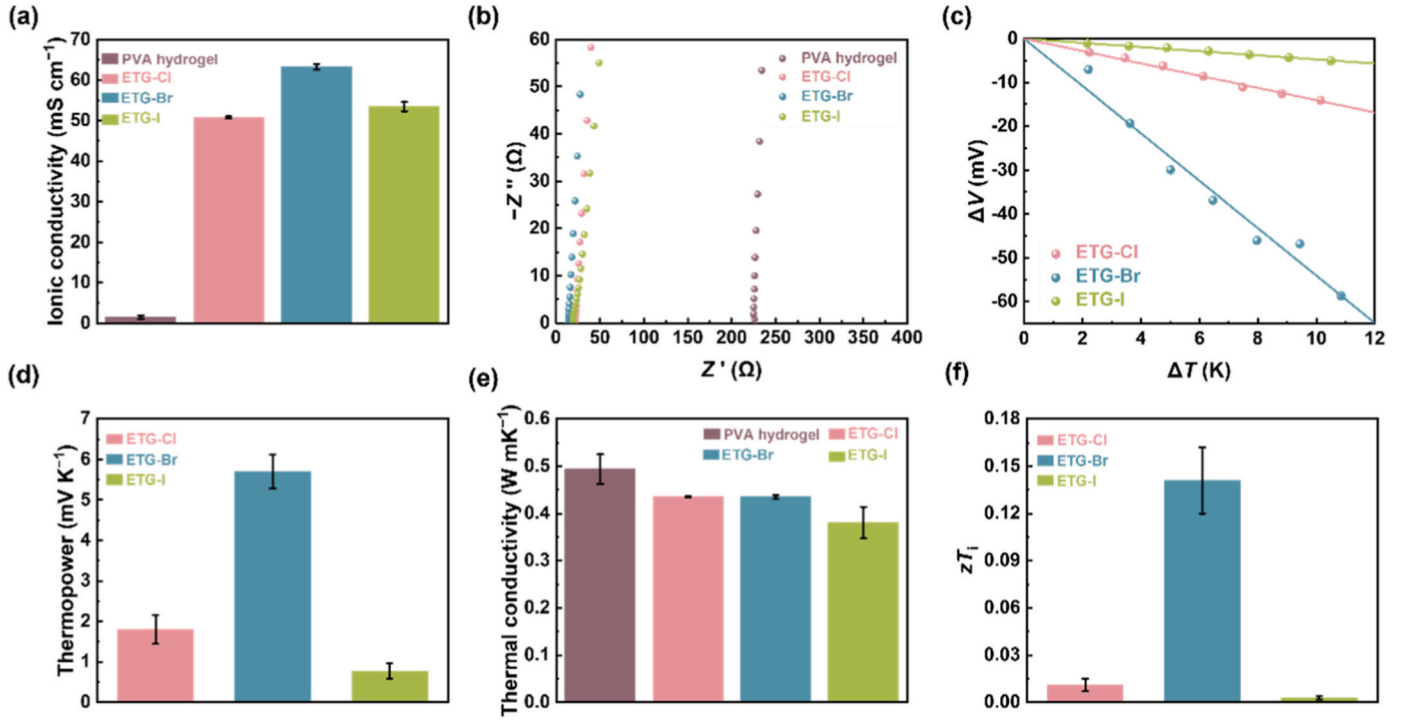


Fig. 5. Thermoelectric properties of the PVA hydrogel and eutectogels: (a) ionic conductivity, (b) Nyquist plots from EIS analysis, (c) ΔV - ΔT plot, (d) thermopower, (e) thermal conductivity, and (f) zT_i value.

3.4. Small-angle x-ray scattering characterization

The nanostructural organization of the pristine PVA hydrogel and various ETGs is systematically revealed by the small-angle X-ray scattering (SAXS) results in Fig. 4(a-d) and the corresponding quantitative fitting parameters in Table S3. Here, the hierarchical architecture of the gel network is analyzed by using the Beaucage model, which is an established multiscale approach for interpreting a variety of polymer morphologies, ranging from random coils to complex aggregated structures [39,40]. The Beaucage model combines Guinier and power-law scattering contributions, and is expressed as Eq. (1):

$$I(q) \cong I_{bkg} + \sum_{i=1}^N \left\{ G_i \exp\left(-\frac{q^2 R_{gi}^2}{3}\right) + B_i \exp\left(-\frac{q^2 R_{g(i+1)}^2}{3}\right) \times \left\{ \frac{\left[\text{erf}\left(\frac{q R_{gi}}{\sqrt{6}}\right)\right]^3}{q} \right\}^{P_i} \right\} \quad (1)$$

where G_i is the Guinier prefactor, B_i is the power-law coefficient, R_{gi} is the radius of gyration, which characterizes the spatial distribution of scattering domains, P_i is the fractal dimension, and the subscript i distinguishes between different hierarchical levels of structural organization. In this analysis, two distinct structural hierarchies are analyzed, including: the 1st level ($i = 1$), which spans the low- q range of 0.0015–0.01 Å⁻¹ and corresponds to global and large-scale clusters, and the 2nd level ($i = 2$), which covers the high- q range of 0.01–0.1 Å⁻¹ and reflects local or secondary structural features.

The agglomerate architecture is schematically represented in Fig. 4(e) as a mass-fractal network, where large clusters with gyration radius R_{g1} are assembled from the hierarchical aggregation of secondary particles characterized by gyration radius R_{g2} . These secondary particles are composed of polymer chains, and the conformational states and packing characteristics are examined across different hierarchical levels of the

structure [41]. At 1st level, R_{g1} progressively increases from 114.6 nm for PVA hydrogel to 116.2, 118.7, and 161.2 nm for ETG-Cl, ETG-Br, ETG-I, respectively. This trend indicates that the incorporation of increasingly chaotropic halide anions induces a substantial expansion of the polymer network. The increase in R_{g1} results from the disruption of water's hydrogen bonding by chaotropic anions, which reduces hydrophobic effects of the DES and enables the PVA chains to adopt a more extended conformation. As a result, the PVA chains undergo conformational changes and extension, thereby enlarging the overall cluster dimensions. Similarly, at the 2nd structural level, the R_{g2} increases from 11.2 nm in the PVA hydrogel to 15.6 nm in ETG-I, thereby indicating parallel expansion of local polymer domains as the strength of halide-induced disruption increases. These findings indicate that both global aggregates and nanoscale domains become progressively more expanded in the presence of more chaotropic halides.

The fractal dimensions (P_1 and P_2) derived from the Beaucage fits (Table S3) quantify the mass fractal characteristics of the global and local structures. Notably, the ETG-I exhibits lowest fractal dimensions ($P_1 = 2.0$, $P_2 = 2.6$), which is consistent with a looser and rougher fractal morphology. Conversely, the ETG-Cl ($P_1 = 3.0$, $P_2 = 3.2$) and ETG-Br ($P_1 = 2.9$, $P_2 = 3.3$) display higher fractal dimensions, thereby indicating more compact and smoother hierarchical structures. This behavior can be explained by the weaker hydration of I⁻ anions (the most chaotropic of the three halides) and their the disruption of the hydrogen-bonding network of water. The resulting environment facilitates greater PVA chain expansion and disrupts ordered packing. These observations highlight the important role of halide anion identity in modulating the hierarchical architecture of PVA-based gel networks. The progression from Cl⁻ to I⁻ leads to increasing structural expansion at both global and local scales, thereby reflecting the fundamental influence of ion-polymer interactions on gel nanostructure.

The thermal stability of each sample under relevant operating conditions is revealed by the temperature-dependent SAXS measurements in Fig. S7. Here, all of the samples retain consistent SAXS profiles at temperatures of up to 40 °C, thereby confirming the structural integrity of the gels within the temperature range used for thermoelectric

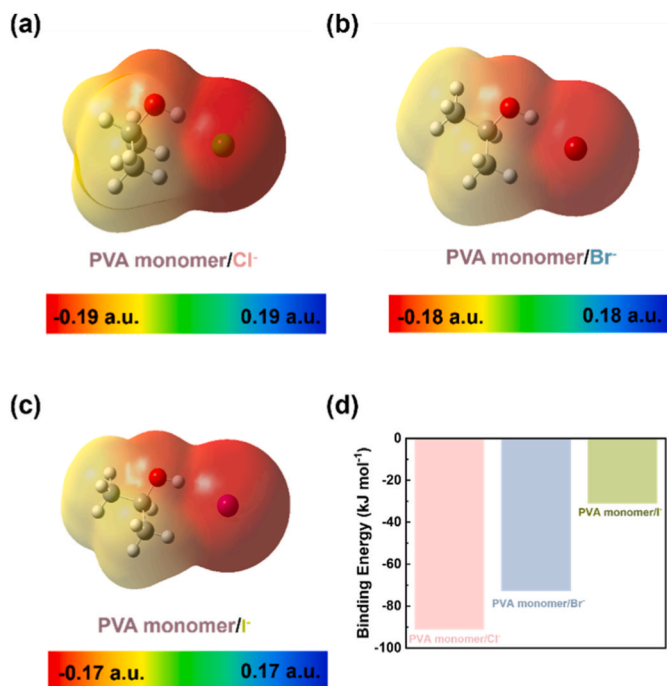


Fig. 6. Electrostatic potential (ESP) maps of (a) PVA monomer/ Cl^- , (b) PVA monomer/ Br^- , and (c) PVA monomer/ I^- . (d) Calculated binding energies between halide anions and PVA monomer obtained from DFT analysis.

characterization. Accordingly, all subsequent thermoelectric measurements were conducted at or below 40 °C to preserve the native nanostructures and ensure accurate evaluation of the material performance.

3.5. Thermoelectric property analysis

The thermoelectric performances of the PVA hydrogel and various ETGs are evaluated by the following ionic conductivity (σ_i), thermopower (S_i), thermal conductivity (κ) measurements, along with the corresponding ionic figure of merit (zT_i) values, as summarized in Table S4. These metrics provide a comprehensive assessment of the ionic thermoelectric energy conversion capabilities of the materials. The ionic conductivities of the various samples are derived from the electrochemical impedance spectroscopy (EIS) and corresponding Nyquist plots in Fig. 5(a and b), respectively. Here, it can be seen that the incorporation of a DES leads to a significant increase in σ_i , from 1.52 mS cm^{-1} for the pristine PVA hydrogel to 50.74, 63.33, and 53.44 mS cm^{-1} for the ETG-Cl, ETG-Br, and ETG-I, respectively. Among the ETGs, the relatively low conductivity of the ETG-Cl can be attributed to the higher viscosity of the ChCl:Gly system (Fig. S8), which restricts ion mobility [42]. Meanwhile, the larger ionic radius of I^- introduces steric hindrance that impedes migration, thereby resulting in elevated resistance and, hence, only a moderate increase in σ_i relative to that of the ETG-Cl [43]. By contrast, the ETG-Br exhibits the highest conductivity of all, thereby suggesting a favorable combination of relatively low viscosity in the ChBr:Gly system and the moderate ionic size of Br^- , each of which promote efficient ion transport. These results demonstrate that both viscosity and steric factors play critical roles in governing ionic transport within ETG matrices.

The thermopower or ionic Seebeck coefficient (S_i), quantifies the voltage generated per unit temperature difference, and is defined by Eq. (2):

$$S_i = \frac{\Delta V}{\Delta T} = \frac{V(T_H) - V(T_C)}{T_H - T_C} \quad (2)$$

where $V(T_H)$ and $V(T_C)$ represent the respective voltages at the hot and

cold ends, and $\Delta T = |T_H - T_C|$ is the applied temperature gradient between these two ends. Thus, the S_i values can be obtained from the slopes of the $\Delta V - \Delta T$ plots in Fig. 5(c). As shown in Fig. 5(d), the ETG-Br exhibits the highest S_i of 5.70 mV K^{-1} , followed by the ETG-Cl at 1.80 mV K^{-1} and the ETG-I at 0.78 mV K^{-1} . The magnitude of S_i is strongly influenced by the differential transport of cations and anions, which in turn depends on ion-polymer interactions with the matrix.

To further elucidate these effects, electrostatic potential (ESP) mapping and density functional theory (DFT) calculations were performed to visualize charge distributions and assess potential halide-PVA binding characteristics. Despite possible interference from surrounding water molecules, the ESP maps in Fig. S9 indicate that halide ions with negative electrostatic potential preferentially interact with the positively polarized hydroxyl groups on the PVA monomer. Meanwhile, the DFT results in Fig. 6 reveal negative binding energies of -91.07, -72.66, and -30.97 kJ mol^{-1} between the PVA monomer and Cl^- , Br^- , and I^- , respectively. By contrast, the DFT results in Fig. S10 indicate a positive binding energy of 174.78 kJ mol^{-1} between Ch^+ and the PVA monomer, thereby indicating that the combined system is energetically less stable than the isolated components (i.e., their interaction is weak and unfavorable) [44]. It should be noted that these DFT calculations were performed using a simplified cluster model containing PVA, Ch^+ , and halide anions to capture the dominant coordination features. While the actual eutectogel environment also includes glycerol and water molecules, previous studies have shown that such solvent species primarily induce minor modulation through hydrogen-bond competition or dielectric screening rather than fundamentally altering the intrinsic binding hierarchy [45]. Accordingly, while the absolute binding strength may be slightly adjusted in the presence of glycerol and water, the relative halide-PVA affinity trend ($\text{Cl}^- > \text{Br}^- > \text{I}^-$) remains reliable and consistent with the experimental thermoelectric behavior of the ETGs. Consequently, Ch^+ is more likely to remain mobile within the matrix, thereby facilitating its diffusion under a thermal gradient and contributing to the observed p-type thermoelectric behavior in the ETGs. In terms of different halide ions, although Cl^- demonstrates the strongest binding interaction with PVA monomer, its effect on S_i is limited by the high viscosity of the ChCl:Gly medium. This elevated viscosity increases the driving force required for ion transport, thereby restricting the mobility of Ch^+ and suppressing differential ion migration. By contrast, I^- displays the weakest binding due to its large ionic radius and low charge density, thus resulting in insufficient ion-gel interactions and minimal ion-selective diffusion under a thermal gradient, which leads to the lowest S_i value. Meanwhile, the ETG-Br achieves the most favorable balance between polymer interaction strength and ionic mobility. The moderate binding energy of Br^- supports selective association with the PVA matrix, while the lower viscosity of the ChBr:Gly system facilitates effective ion transport. This synergistic effect enables efficient differential ion diffusion, thereby resulting in the highest S_i value among the tested samples.

As shown in Fig. 5(e), the thermal conductivity (κ) also varies among the samples. As the polymer matrix is the primary medium for phonon transport, structural changes induced by halide anions exert a direct influence on κ . Based on the SAXS analysis, I^- induces the greatest disruption in polymer packing due to its strong chaotropic nature, thus resulting in a looser, more disordered structure. This effectively impedes thermal transport and yields the lowest κ value of 0.38 $\text{W m}^{-1} \text{K}^{-1}$ for the ETG-I. By comparison, the ETG-Br and ETG-Cl each exhibit a slightly higher κ value of 0.46 $\text{W m}^{-1} \text{K}^{-1}$, which is attributed to their relatively more ordered internal structures. Meanwhile, the efficiency of each ionic thermoelectric gel is ultimately quantified by the dimensionless ionic figure of merit (zT_i), as expressed in Eq. (3):

$$zT_i = \frac{\sigma_i S_i^2 T}{\kappa} \quad (3)$$

As shown in Fig. 5(f), the ETG-Br achieves the highest zT_i value of 0.14 at room temperature, surpassing those of the ETG-Cl and ETG-I.

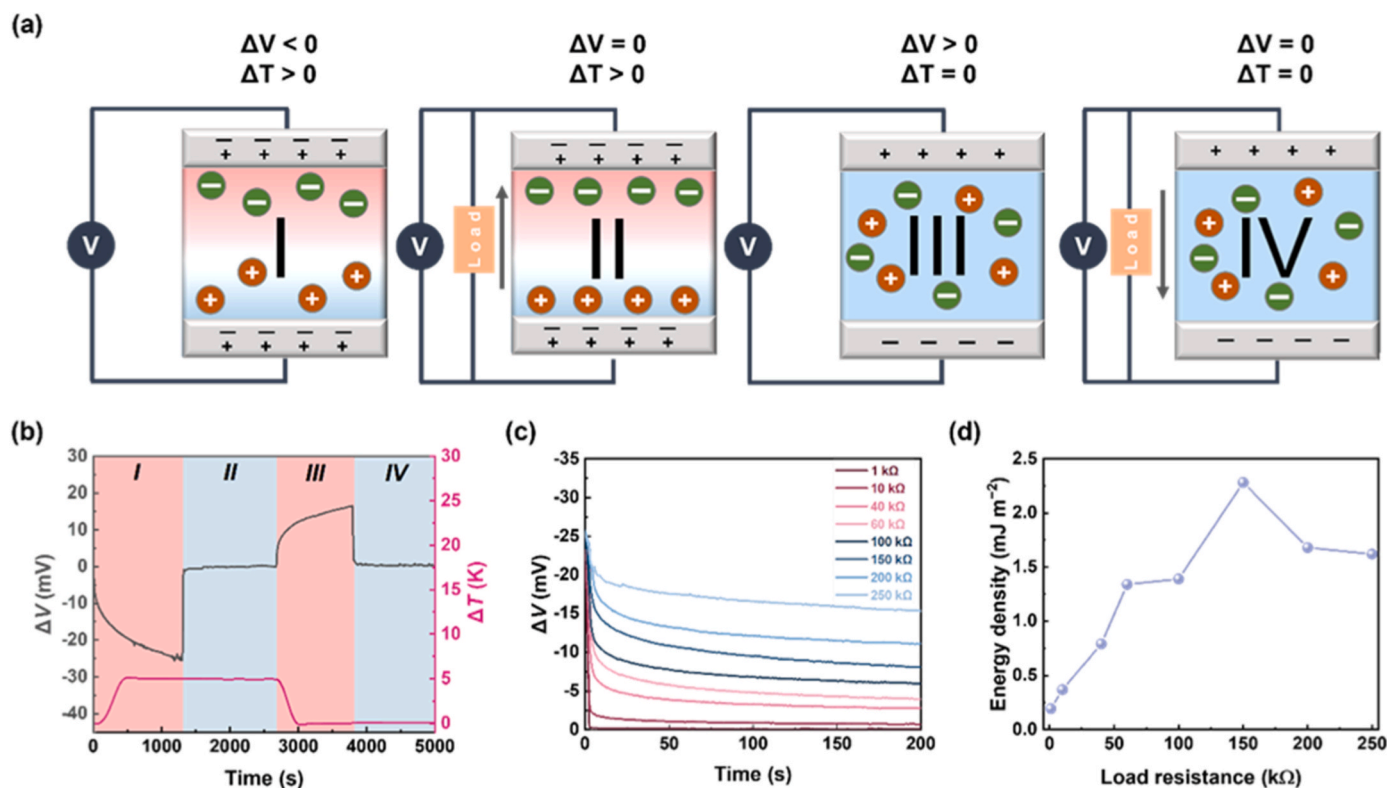


Fig. 7. (a) Conceptual diagram illustrating the four-stages working mechanism of the ionic thermoelectric capacitor. (b) Voltage-time response under a 5 K temperature gradient and a 10 kΩ external load, correlated with the four operational stages. (c) Voltage decay curves and (d) calculated energy density for various external resistances.

This enhanced performance is attributed to the optimal balance of properties in the Br⁻-based system, including moderate viscosity, favorable halide-polymer interactions, and efficient ionic mobility asymmetry between cations and anions. Furthermore, as summarized in Table S2, the addition of a HBA in the ETG-Br formulation enables the crosslinker-free gel to achieve a comparable thermoelectric performance to that of typical ETGs with chemical cross-linkers. These results highlight the potential of tailored halide selection and eutectic composition as effective strategies for optimizing DES-based thermoelectric materials without relying on permanent chemical crosslinking.

3.6. Ionic thermoelectric capacitor

To further evaluate the thermoelectric capacitive performance of the ETG-Br, an ionic thermoelectric capacitor device was fabricated by sandwiching the ETG-Br gel between two platinum electrodes. The operating principle of this device is illustrated in Fig. 7(a and b), which depict a four-stage thermal charging-discharging cycle. In the first stage, the application of a 5 K temperature gradient induces thermodiffusion of ionic species within the gel. Due to the differences in mobility between the cations and anions, selective ionic diffusion occurs under a temperature gradient, thus resulting in charge separation and the accumulation of ions near the electrodes. This leads to the formation of an electric double layer at the electrode-gel interface [46]. Consequently, an open-circuit voltage develops, reaching approximately -25.2 mV. In the second stage, connection of a 10 kΩ external load initiates a rapid voltage decay as charge flows through the external circuit and electrons and holes are injected into the respective electrodes to compensate for the thermally accumulated cations and anions [47]. In the third stage, after removal of both the thermal gradient and the external resistor, the ion species within the gel tend to return to their initial homogeneous distribution. Consequently, electrons and holes remain trapped at the respective electrodes, thereby yielding a voltage of opposite polarity

relative to the first stage. Finally, in the fourth stage, reintroducing the external resistor leads to gradual neutralization of the accumulated charges, which causes the voltage difference to decay back toward zero [48,49].

To systematically investigate the charge-discharge dynamics, a range of external resistances was applied during the second stage, with the corresponding responses presented in Fig. 7(c). The results indicate that increasing the external resistance progressively slows the rate of voltage decay. This behavior is because a larger resistance limits the current flow, thereby reducing the rate at which stored charges are dissipated and allowing the voltage to be maintained over a longer duration. These findings highlight the tunability of the discharge behavior through impedance matching.

The energy storage performance of the device can be quantified by calculating the energy density (E), using Eq. (4) [50].

$$E = \frac{\int U^2 / R dt}{A} \quad (4)$$

where U denotes the applied voltage, R is the external resistance, and A represents the cross-sectional area of the gel. As shown in Fig. 7(d), optimal impedance matching is achieved with an external resistance of 150 kΩ, thus resulting in a maximum energy density of 2.3 mJ m⁻². This result demonstrates the promising potential of the ETG-Br-based ionic thermoelectric capacitor for energy storage applications.

3.7. Wearable device application

To demonstrate its practical feasibility for real-world applications, the optimal ETG-Br formulation was integrated into a prototype thermoelectric device and tested under conditions that were designed to mimic wearable application scenarios. Specifically, the device was configured such that its hot side was placed in direct contact with the

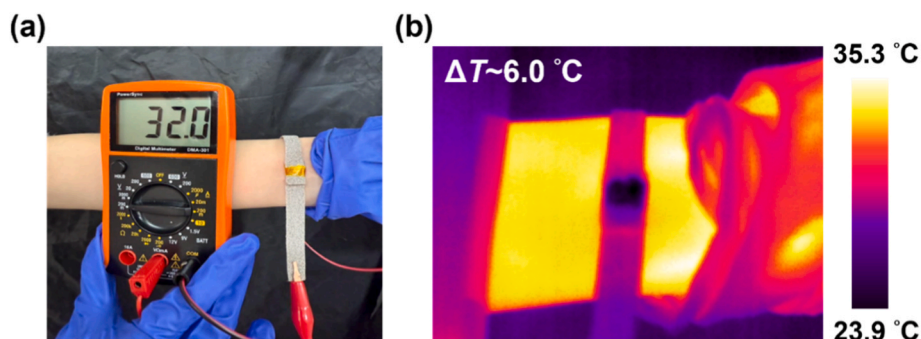


Fig. 8. (a) Schematic representation of the wearable thermoelectric device placed on the wrist, generating thermal voltage from a wrist-environment temperature gradient (~ 6.0 °C). (b) Infrared thermal images of the device during operation.

human wrist, while the cold side remained exposed to ambient air, thereby establishing a temperature gradient across the gel and enabling thermoelectric voltage generation. To ensure reliable and conformal electrical contact with the wrist, flexible nickel-platinum electrodes were employed at both the hot and cold interfaces, thereby providing stable and low-resistance electrical connections throughout the testing process. As illustrated in Fig. 8(a and b), this wearable configuration enables the device to generate an open-circuit thermoelectric voltage of 32.0 mV under a modest temperature difference of only 6 °C. These results provide compelling evidence for the potential of ETG-Br as a functional material for skin-conformal, environmentally friendly, low-grade heat harvesting thermoelectric devices. Moreover, the demonstrated performance underscores the potential of the DES in the development of efficient thermoelectric materials. The ETG-Br achieves a well-balanced combination of viscosity, halide-polymer interactions, and ionic size, which collectively promote selective ion diffusion and enhance the thermoelectric performance. These attributes position the ETG-Br as a promising candidate for next-generation wearable energy-harvesting applications. Future studies could explore the integration of ETG-Br into a wider range of energy-harvesting scenarios beyond wearable devices, such as low-grade industrial waste heat recovery or smart building applications. Additionally, further tuning of DES composition and polymer matrix could enable optimization of ion transport and mechanical properties, offering versatile strategies for designing sustainable and efficient thermoelectric materials.

4. Conclusions

Herein, an environmentally friendly eutectogel (ETG) was successfully developed by directly blending polyvinyl alcohol (PVA) with a deep eutectic solvent (DES), thereby promoting material sustainability and facile processability. Glycerol served as the hydrogen bond donor (HBD), while choline chloride (ChCl), choline bromide (ChBr), and choline iodide (ChI) acted as hydrogen bond acceptors (HBAs) to form the various DES systems. The specific identity of the HBA was found to markedly influence the polymer conformation, ion transport behavior, and thermoelectric properties of the ETG. Specifically, the distinct chaotropic characteristics of the halide anions modulated the DES microstructure by altering the hydrogen bonding network and inducing conformational transitions in the PVA chains. Spectroscopic and scattering analyses revealed that I^- , with the strongest chaotropic effect, most effectively disrupted hydrogen bonding and reduced the crystallinity. However, the large ionic radius of I^- hindered the ion mobility. Meanwhile, Cl^- exhibited strong binding interactions with the PVA monomer, along with enhanced ion selectivity, but limited the ionic transport due to the high viscosity of the ChCl-based system. Among the evaluated systems, the ChBr-based DES achieves an optimal balance between ion mobility and polymer coordination, providing distinct structural and transport advantages over the conventional ChCl-based system. Consequently, the ChBr-based ETG (designated as ETG-Br)

exhibited the highest ionic conductivity and thermopower of 63.33 mS cm^{-1} and 5.70 mV K^{-1} , respectively. Additionally, the ETG-Br maintained robust mechanical stability, supporting a consistent and reliable thermoelectric performance. When implemented in an ionic thermoelectric capacitor, the ETG-Br achieved an areal energy density of 2.3 mJ m^{-2} and generated an output voltage of 32.0 mV under a 6 °C temperature gradient in a wearable device configuration. Overall, these findings establish the ChBr-based DES system as a promising and well-balanced design for thermoelectric ETGs, offering a synergistic combination of ionic conductivity, thermopower, mechanical integrity, and sustainable processability for heat-harvesting applications.

CRediT authorship contribution statement

Yu-Syuan Jheng: Writing – review & editing, Writing – original draft, Visualization, Methodology, Investigation, Formal analysis, Data curation, Conceptualization. **Ching-Chieh Hsu:** Formal analysis, Conceptualization. **Shao-Huan Hong:** Formal analysis, Conceptualization. **Chi-Wei Hsu:** Formal analysis, Data curation. **Shiao-Wei Kuo:** Formal analysis, Conceptualization. **Chia-Hsin Wang:** Resources. **U-Ser Jeng:** Resources. **Shih-Huang Tung:** Writing – review & editing, Formal analysis. **Cheng-Liang Liu:** Writing – review & editing, Supervision, Funding acquisition, Conceptualization.

Declaration of competing interest

The authors declare that they have no known competing financial interests or personal relationships that could have appeared to influence the work reported in this paper.

Acknowledgments

The authors gratefully acknowledge financial support from the National Science and Technology Council (NSTC), Taiwan, through the 2030 Cross-Generation Young Scholars Program (113-2628-E-002-028), and the Academic Research-Career Development Project of National Taiwan University (NTU114L7817). Additional support was provided by the Advanced Research Center for Green Materials Science and Technology under the Featured Area Research Center Program, funded through the Ministry of Education's Higher Education Sprout Project (114L9006). The authors also appreciate the access to beamtime at Beamline TPS 13A and TLS 24A of the National Synchrotron Radiation Research Center (NSRRC), Taiwan. The authors gratefully thank Ms. Ya-Yun Yang for her assistance in SEM experiments conducted at the Instrumentation Center of National Taiwan University, supported by the NSTC. List all funding that support this work.

Appendix A. Supplementary data

Supplementary data to this article can be found online at <https://doi.org/10.1016/j.mtener.2025.102105>.

[org/10.1016/j.mtener.2025.102105](https://doi.org/10.1016/j.mtener.2025.102105).

Data availability

Data will be made available on request.

References

- [1] H. Zhou, H. Inoue, M. Ujita, T. Yamada, Advancement of electrochemical thermoelectric conversion with molecular technology, *Angew. Chem. Int. Ed.* 62 (2) (2023) e202213449, <https://doi.org/10.1002/anie.202213449>.
- [2] C.-Y. Lee, Y.-T. Lin, S.-H. Hong, C.-H. Wang, U.S. Jeng, S.-H. Tung, C.-L. Liu, Mixed ionic-electronic conducting hydrogels with carboxylated carbon nanotubes for high performance wearable thermoelectric harvesters, *ACS Appl. Mater. Interfaces* 15 (48) (2023) 56072–56083, <https://doi.org/10.1021/acsami.3c09934>.
- [3] C. Zhang, X.-L. Shi, Q. Liu, Z.-G. Chen, Hydrogel-Based functional materials for thermoelectric applications: progress and perspectives, *Adv. Funct. Mater.* 34 (51) (2024) 2410127, <https://doi.org/10.1002/adfm.202410127>.
- [4] C.-G. Han, X. Qian, Q. Li, B. Deng, Y. Zhu, Z. Han, W. Zhang, W. Wang, S.-P. Feng, G. Chen, W. Liu, Giant thermopower of ionic gelatin near room temperature, *Science* 368 (6495) (2020) 1091–1098, <https://doi.org/10.1126/science.aaz5045>.
- [5] Y.-C. Hsiao, L.-C. Lee, Y.-T. Lin, S.-H. Hong, K.-C. Wang, S.-H. Tung, C.-L. Liu, Stretchable polyvinyl alcohol and sodium alginate double network ionic hydrogels for low-grade heat harvesting with ultrahigh thermopower, *Mater. Today Energy* 37 (2023) 101383, <https://doi.org/10.1016/j.mtener.2023.101383>.
- [6] S.-T. Kao, C.-C. Hsu, S.-H. Hong, U.-S. Jeng, C.-H. Wang, S.-H. Tung, C.-L. Liu, Host-Guest complexation of α -Cyclodextrin and triiodide ions for enhanced performance of ionic thermoelectric capacitors, *Adv. Energy Mater.* 15 (15) (2025) 2405502, <https://doi.org/10.1002/aenm.202405502>.
- [7] H. Cheng, J. Ouyang, Soret effect of ionic liquid gels for thermoelectric conversion, *J. Phys. Chem. Lett.* 13 (46) (2022) 10830–10842, <https://doi.org/10.1021/acs.jpclett.2c02645>.
- [8] C.-Y. Lee, S.-H. Hong, C.-L. Liu, Recent progress in polymer gel-based ionic thermoelectric devices: materials, methods, and perspectives, *Macromol. Rapid Commun.* 46 (8) (2025) 2400837, <https://doi.org/10.1002/marc.202400837>.
- [9] L.-C. Lee, K.-T. Huang, Y.-T. Lin, U.-S. Jeng, C.-H. Wang, S.-H. Tung, C.-J. Huang, C.-L. Liu, A pH-Sensitive stretchable zwitterionic hydrogel with bipolar thermoelectricity, *Small* 20 (24) (2024) 2311811, <https://doi.org/10.1002/sml.202311811>.
- [10] S. Sun, M. Li, X.-L. Shi, Z.-G. Chen, Advances in ionic thermoelectrics: from materials to devices, *Adv. Energy Mater.* 13 (9) (2023) 2203692, <https://doi.org/10.1002/aenm.202203692>.
- [11] Y.-H. Pai, J. Tang, Y. Zhao, Z. Liang, Ionic organic thermoelectrics with impressively high thermopower for sensitive heat harvesting scenarios, *Adv. Energy Mater.* 13 (1) (2023) 2202507, <https://doi.org/10.1002/aenm.202202507>.
- [12] N. Ben Halima, Poly(vinyl alcohol): review of its promising applications and insights into biodegradation, *RSC Adv.* 6 (46) (2016) 39823–39832, <https://doi.org/10.1039/C6RA05742J>.
- [13] L.-C. Lee, S.-H. Hong, M.-S. Kim, U.S. Jeng, C.-H. Wang, S.-H. Tung, K.H. Lee, C.-L. Liu, Enhanced thermoelectric performance of PVA-Based ionogels: tailoring crystallinity via additives for advanced waste heat recovery, *ACS Appl. Mater. Interfaces* 17 (26) (2025) 38545–38557, <https://doi.org/10.1021/acsami.5c08724>.
- [14] Y. Hui, R. Liu, T. Sun, L. Li, Y. Gong, Z. Xiao, A. Xu, X. Wei, Engineering Robust conductive Hydrogel sensors with enhanced mechanical properties and practical applicability, *Macromolecules* 57 (10) (2024) 4737–4746, <https://doi.org/10.1021/acs.macromol.3c02328>.
- [15] G.B. McKenna, F. Horkay, Effect of crosslinks on the thermodynamics of poly(vinyl alcohol) hydrogels, *Polymer* 35 (26) (1994) 5737–5742, [https://doi.org/10.1016/S0032-3861\(05\)80049-7](https://doi.org/10.1016/S0032-3861(05)80049-7).
- [16] H. Cheng, X. He, Z. Fan, J. Ouyang, Flexible quasi-solid state ionogels with remarkable seebeck coefficient and high thermoelectric properties, *Adv. Energy Mater.* 9 (32) (2019) 1901085, <https://doi.org/10.1002/aenm.201901085>.
- [17] W. Zhao, Y. Zheng, M. Jiang, T. Sun, A. Huang, L. Wang, W. Jiang, Q. Zhang, Exceptional n-type thermoelectric ionogels enabled by metal coordination and ion-selective association, *Sci. Adv.* 9 (43) (2023) eadk2098, <https://doi.org/10.1126/sciadv.adk2098>.
- [18] J.K.U. Ling, K. Hadinoto, Deep eutectic solvent as green solvent in extraction of biological macromolecules: a review, *Int. J. Mol. Sci.* 23 (6) (2022) 3381, <https://doi.org/10.3390/ijms23063381>.
- [19] H. Wu, J. Song, N. Gao, X. Pang, Y. Li, Z. Xu, X. Yu, High performance eutectogel-based thermocell with a wide operating temperature range through a water-containing deep eutectic solvent strategy, *Chem. Eng. J.* 505 (2025) 159714, <https://doi.org/10.1016/j.cej.2025.159714>.
- [20] P.A. Mercadal, A. González, A. Beloqui, L.C. Tomé, D. Mecerreyes, M. Calderón, M. L. Picchio, Eutectogels: the multifaceted soft ionic materials of tomorrow, *JACS Au* 4 (10) (2024) 3744–3758, <https://doi.org/10.1021/jacsau.4c00677>.
- [21] Y. Zhao, H. Cheng, Y. Li, J. Rao, S. Yue, Q. Le, Q. Qian, Z. Liu, J. Ouyang, Quasi-solid conductive gels with high thermoelectric properties and high mechanical stretchability consisting of a low cost and green deep eutectic solvent, *J. Mater. Chem. A* 10 (8) (2022) 4222–4229, <https://doi.org/10.1039/D1TA09707E>.
- [22] Y. Chen, G. Hong, L. Li, Q. Qu, G. Li, J. Wu, L. Ge, Enlightening thermoelectric mastery: Bio-inspired cellulose gel containing eco-friendly deep eutectic solvents, *Chem. Eng. J.* 483 (2024) 149344, <https://doi.org/10.1016/j.cej.2024.149344>.
- [23] Y. Wang, Y. Wang, L. Yan, Deep eutectic solvent-induced microphase separation and entanglement of PVA chains for tough and reprocessable eutectogels for sensors, *Langmuir* 38 (40) (2022) 12189–12197, <https://doi.org/10.1021/acs.langmuir.2c01770>.
- [24] D. Motta, S. Mondahchouo, S. Nejrotti, C. Pontremoli, C. Barolo, A. Damin, M. Bonomo, Glycerol-based deep eutectic solvents for efficient and reversible iodine uptake from vapour phase, *Commun. Chem.* 8 (1) (2025) 178, <https://doi.org/10.1038/s42004-025-01575-2>.
- [25] G. Mastellone, N.M. Abbasi, C. Cagliero, J.L. Anderson, New class of Tunable Choline bromide-based hydrophobic deep eutectic solvents for the extraction of bioactive compounds of varying polarity from a plant matrix, *ACS Sustainable Chem. Eng.* 11 (17) (2023) 6665–6675, <https://doi.org/10.1021/acssuschemeng.3c00185>.
- [26] M.D.C.L. Cheng-Tan, A.N. Nguyen, C.T. Gordon, Z.A. Wood, Y. Manjarrez, M. E. Fieser, Choline halide-based deep eutectic solvents as biocompatible catalysts for the alternating copolymerization of epoxides and cyclic anhydrides, *ACS Sustainable Chem. Eng.* 12 (19) (2024) 7246–7255, <https://doi.org/10.1021/acssuschemeng.3c06766>.
- [27] T.H. Vo, P.K. Lam, R.-m. Chuang, F.-K. Shieh, Y.-J. Sheng, H.-K. Tsao, One-step, additive-free fabrication of highly stretchable and ultra-tough physical polyvinyl alcohol-based eutectogels for strain sensors, *Chem. Eng. J.* 493 (2024) 152877, <https://doi.org/10.1016/j.cej.2024.152877>.
- [28] X. Lyu, Z. Lin, C. Huang, X. Zhang, Y. Lu, Z.-Z. Luo, P. Zhou, Z. Zou, Tough and elastic hydrogel thermocells for heat energy utilization, *Chem. Eng. J.* 493 (2024) 152887, <https://doi.org/10.1016/j.cej.2024.152887>.
- [29] M.J. Ramazani-Harandi, M.J. Zohuriaan-Mehr, A.A. Yousefi, A. Ershad-Langroudi, K. Kabiri, Rheological determination of the swollen gel strength of superabsorbent polymer hydrogels, *Polym. Test.* 25 (4) (2006) 470–474, <https://doi.org/10.1016/j.polymeresting.2006.01.011>.
- [30] C. Norioka, Y. Inamoto, C. Hajime, A. Kawamura, T. Miyata, A universal method to easily design tough and stretchable hydrogels, *NPG Asia Mater.* 13 (1) (2021) 34, <https://doi.org/10.1038/s41427-021-00302-2>.
- [31] K. Fan, W. Wei, Z. Zhang, B. Liu, W. Feng, Y. Ma, X. Zhang, Highly stretchable, self-healing, and adhesive polymeric eutectogel enabled by hydrogen-bond networks for wearable strain sensor, *Chem. Eng. J.* 449 (2022) 137878, <https://doi.org/10.1016/j.cej.2022.137878>.
- [32] H. Wu, Z. Pang, L. Ji, X. Pang, Y. Li, X. Yu, Strong adhesive, high conductive and environmentally stable eutectogel based on “water in deep eutectic solvent”: ultrasensitive flexible temperature and strain sensors, *Chem. Eng. J.* 497 (2024) 154883, <https://doi.org/10.1016/j.cej.2024.154883>.
- [33] Y. Wang, J. Wang, Z. Ma, L. Yan, A highly conductive, Self-Recoverable, and strong eutectogel of a deep eutectic solvent with polymer crystalline domain regulation, *ACS Appl. Mater. Interfaces* 13 (45) (2021) 54409–54416, <https://doi.org/10.1021/acsami.1c17442>.
- [34] B. Huang, W. Liu, Y. Lan, Y. Huang, L. Fu, B. Lin, C. Xu, Highly ion-conducting, robust and environmentally stable poly(vinyl alcohol) eutectic gels designed by natural polyelectrolytes for flexible wearable sensors and supercapacitors, *Chem. Eng. J.* 480 (2024) 147888, <https://doi.org/10.1016/j.cej.2023.147888>.
- [35] X. Wang, C. Qiao, K. Song, S. Jiang, J. Yao, Hofmeister effect on the viscosity properties of gelatin in dilute solutions, *Colloids Surf., B* 206 (2021) 111944, <https://doi.org/10.1016/j.colsurfb.2021.111944>.
- [36] Z. Yang, Z. Lin, L. Gao, Chaotropic salt dispersion enables room-temperature synthesis of high-purity polyvinyl butyral, *Ind. Eng. Chem. Res.* 63 (19) (2024) 8591–8600, <https://doi.org/10.1021/acs.iecr.4c00637>.
- [37] C. Yin, J. Sun, C. Cui, K.-K. Yang, L.-Y. Shi, Y. Li, Chaotropic ions mediated polymer gelation for thermal management, *Adv. Sci.* 11 (32) (2024) 2405077, <https://doi.org/10.1002/adv.202405077>.
- [38] L. Zhang, Z. Wang, C. Xu, Y. Li, J. Gao, W. Wang, Y. Liu, High strength graphene oxide/polyvinyl alcohol composite hydrogels, *J. Mater. Chem.* 21 (28) (2011) 10399–10406, <https://doi.org/10.1039/C0JM04043F>.
- [39] G. Beaucage, Approximations leading to a unified Exponential/Power-Law approach to small-angle scattering, *J. Appl. Crystallogr.* 28 (6) (1995) 717–728, <https://doi.org/10.1107/S0021889895005292>.
- [40] O. Shih, K.-F. Liao, Y.-Q. Yeh, C.-J. Su, C.-A. Wang, J.-W. Chang, W.-R. Wu, C.-C. Liang, C.-Y. Lin, T.-H. Lee, C.-H. Chang, L.-C. Chiang, C.-F. Chang, D.-G. Liu, M.-H. Lee, C.-Y. Liu, T.-W. Hsu, B. Mansel, M.-C. Ho, C.-Y. Shu, F. Lee, E. Yen, T.-C. Lin, U. Jeng, Performance of the new biological small- and wide-angle X-ray scattering beamline 13A at the Taiwan Photon Source, *J. Appl. Crystallogr.* 55 (2) (2022) 340–352, <https://doi.org/10.1107/S1600576722001923>.
- [41] A. Taufiq Sunaryono, E.G.R. Putra, A. Okazawa, I. Watanabe, N. Kojima, S. Rugmai, S. Soontaranon, M. Zainuri, Trivikantoro, small-angle X-ray scattering study on PVA/Fe₃O₄ magnetic hydrogels, *Nano* 11 (3) (2016) 1650027, <https://doi.org/10.1142/S1793292016500272>.
- [42] H.-N. Kwon, S.-J. Jang, Y.C. Kang, K.C. Roh, The effect of ILs as co-salts in electrolytes for high voltage supercapacitors, *Sci. Rep.* 9 (1) (2019) 1180, <https://doi.org/10.1038/s41598-018-37322-y>.
- [43] F. Lin, Z. Zuo, B. Cao, H. Wang, L. Lu, X. Lu, Y. Zhu, X. Ji, A comprehensive Study of density, viscosity, and electrical conductivity of choline halide-based eutectic solvents in H₂O, *J. Chem. Eng. Data* 69 (12) (2024) 4362–4376, <https://doi.org/10.1021/acs.jced.4c00218>.
- [44] J.S. Arey, P.C. Aeberhard, I.C. Lin, U. Rothlisberger, Hydrogen bonding described using dispersion-corrected density functional theory, *J. Phys. Chem. B* 113 (14) (2009) 4726–4732, <https://doi.org/10.1021/jp810323m>.
- [45] M. Babu Singh, A. Prajapat, P. Jain, P. Singh, I. Bahadur, N.K. Kaushik, N. Kaushik, K. Kumari, Investigate the ability of deep eutectic solvent (ChCl-glycerol) to sense the sulphur dioxide using density functional theory calculations and molecular

- dynamics simulations, *J. Mol. Liq.* 388 (2023) 122720, <https://doi.org/10.1016/j.molliq.2023.122720>.
- [46] H. Wang, D. Zhao, Z.U. Khan, S. Puzinas, M.P. Jonsson, M. Berggren, X. Crispin, Ionic thermoelectric figure of merit for charging of supercapacitors, *Adv. Electron. Mater.* 3 (4) (2017) 1700013, <https://doi.org/10.1002/aelm.201700013>.
- [47] Q. Le, H. Cheng, J. Ouyang, An ionic thermoelectric capacitor with continuous power generation for heat harvesting, *Chem. Eng. J.* 469 (2023) 143828, <https://doi.org/10.1016/j.cej.2023.143828>.
- [48] D. Zhao, H. Wang, Z.U. Khan, J.C. Chen, R. Gabrielsson, M.P. Jonsson, M. Berggren, X. Crispin, Ionic thermoelectric supercapacitors, *Energy Environ. Sci.* 9 (4) (2016) 1450–1457, <https://doi.org/10.1039/C6EE00121A>.
- [49] X. Yang, Y. Tian, B. Wu, W. Jia, C. Hou, Q. Zhang, Y. Li, H. Wang, High-Performance ionic thermoelectric supercapacitor for integrated energy conversion-storage, *Energy Environ. Mater.* 5 (3) (2022) 954–961, <https://doi.org/10.1002/eem2.12220>.
- [50] Z. Liu, H. Cheng, Q. Le, R. Chen, J. Li, J. Ouyang, Giant thermoelectric properties of ionogels with Cationic doping, *Adv. Energy Mater.* 12 (22) (2022) 2200858, <https://doi.org/10.1002/aenm.202200858>.